Geothermics 63 (2016) 62–73

Contents lists available at ScienceDirect

Geothermics

journal homepage: www.elsevier.com/locate/geothermics

Anomalous distribution of microearthquakes in the Newberry Geothermal Reservoir: Mechanisms and implications

Yi Fang[a,*], Sabine A.M. den Hartog[b], Derek Elsworth[a,b], Chris Marone[b], Trenton Cladouhos[c]

[a] Department of Energy and Mineral Engineering, EMS Energy Institute, and G3 Center, The Pennsylvania State University, University Park, PA 16802, United States
[b] Department of Geosciences, EMS Energy Institute, and G3 Center, The Pennsylvania State University, University Park, PA 16802, United States
[c] AltaRock Energy, Inc., Seattle, WA 98103, United States

ARTICLE INFO

Article history:
Received 23 October 2014
Received in revised form 30 March 2015
Accepted 29 April 2015
Available online 18 June 2015

Keywords:
Fluid-injection-induced microearthquakes
Anomalous distribution
Frictional stability

ABSTRACT

Stimulation of enhanced geothermal system (EGS) reservoirs by fluid injection can enhance the reservoir permeability but may also result in undesired microearthquakes (MEQs). A bimodal depth distribution of fluid-injection-induced MEQs was observed in the 2012 stimulation phase of the Newberry Volcano EGS Demonstration project in Oregon, US. During 7 weeks of hydraulic stimulation of well NWG 55-29, 90% of MEQs occurred in the shallow reservoir (~500 m to ~1800 m), only a few occurred adjacent to the bottom of the open borehole (~2500 to ~3000 m) while almost no seismicity was observed in the intervening interval (~1800 m to ~2500 m). Our analysis of frictional stability using spatial models for fluid pressure diffusion of injected fluids show that the distribution of MEQs is consistent with observed casing damage, and a possible leak at ~700 m, and is inconsistent with migration of fluids from the casing shoe. The role of fluid injection through the ruptured casing is further supported by the analyses of shear failure and pore-pressure diffusion. Finally, the absence of seismicity at intermediate depths is consistent with our laboratory determinations of frictional stability, showing velocity strengthening frictional behavior for samples from intermediate depths, bracketed by velocity neutral and weakening behavior for samples from shallower and greater depths.

1. Introduction

Enhanced Geothermal Systems (EGS) technology has great potential to utilize Earth's vast thermal resources to meet the world's growing need for energy. Since natural-fractured, high-temperature geothermal systems do not necessarily have high permeability for efficient fluid circulation, they are typically stimulated via hydroshearing to recover geothermal energy sustainably and economically. Hydroshearing is achieved by injecting water at a stimulation pressure that is above the local hydrostatic pore-pressures but below the minimum principal stress. This process induces shear failure of preexisting fractures and self-propped Mode II or Mode III cracks, resulting in zones of enhanced permeability in otherwise typically low permeability crystalline rock (Evans et al., 2005; Tester, 2007). The resulting increased heat exchange area and residence time of injected fluids allows these fluids to reach optimum production temperature (Hubbert and Rubey, 1959; Majer and Peterson, 2007), increasing the production of geothermal energy.

A drawback of the hydroshearing technique is that the elevated pore-pressures during fluid injection can induce low magnitude (M_w) microearthquakes (MEQs) in the reservoir where faults are absent in the stimulated region (Bachmann et al., 2011; Majer et al., 2007; Zoback and Harjes, 1997). Additionally, the short-term thermal cooling of the hot reservoir rock and long-term chemical interactions between the rock and the circulating fluid can also induce shear failure or even tensile failure, further enhancing the occurrence of MEQs (Elsworth and Goodman, 1986; Rutqvist et al., 2008). Clearly, the occurrence of MEQs is the result of complex coupled thermal-hydro-mechanical–chemical processes during the development of EGS.

MEQs, while posing a threat to public acceptance of EGS, provide crucial feedback on the progress of subsurface activities in EGS reservoir stimulation (e.g., crack propagation, permeability evolution, and temperature changes (Izadi and Elsworth, 2013; Majer et al., 2007). Particularly, the spatial distribution and timing of

* Corresponding author. Tel.: +1 5622847949.
E-mail address: yi.fang@psu.edu (Y. Fang).

http://dx.doi.org/10.1016/j.geothermics.2015.04.005
0375-6505/

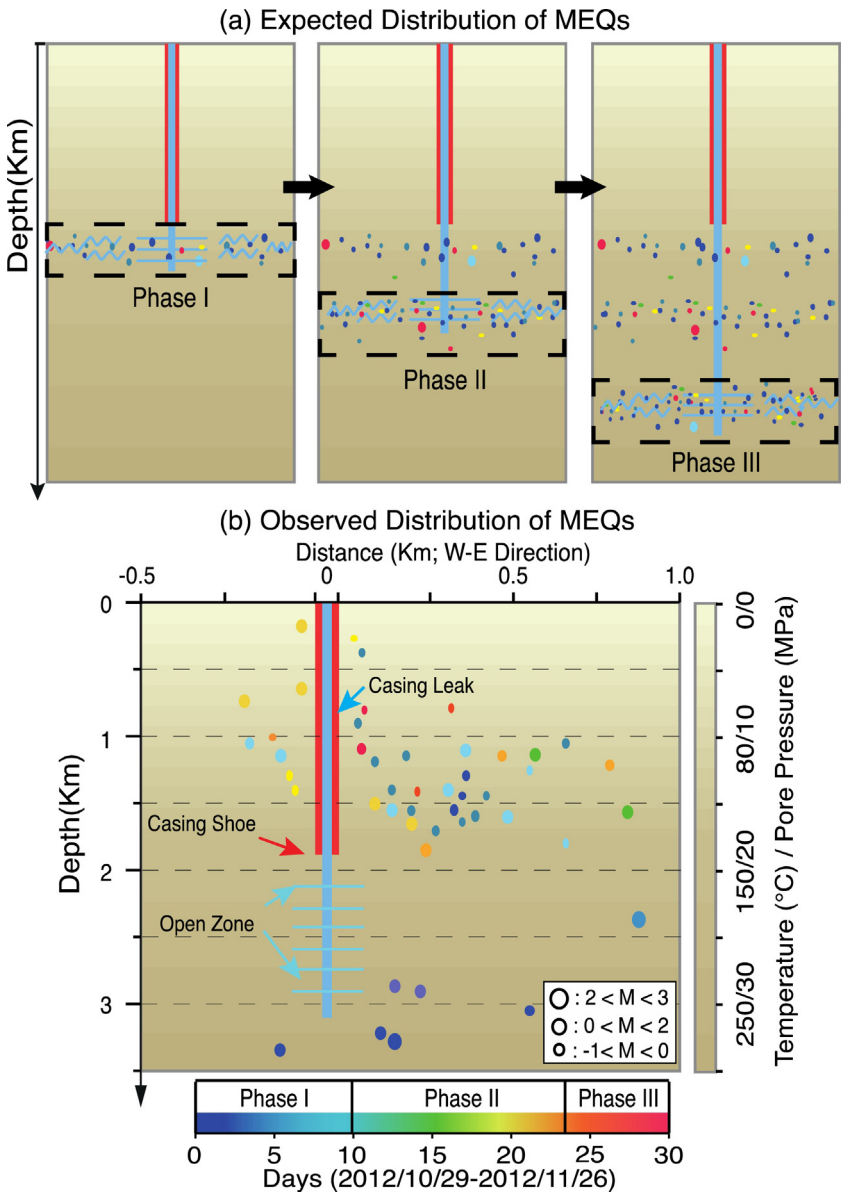

Fig. 1. 2012 stimulation of Well NWG 55-29 was completed through three phases. (a) Expected distribution pattern of MEQs in each of stimulation phase. (b) Observed distribution of MEQs, showing both spatial and temporal anomalies.

MEQs are of significance, potentially providing reliable constraints on the progress and effectiveness of stimulation, guiding optimum production of the reservoir, and ensuring the economic maintenance of reservoir life. Of particular interest in this respect are EGS sites where the seismicity distribution is anomalous. Such an anomalous distribution of MEQs was observed in an EGS Demonstration Project at Newberry Volcano, Oregon that has been operated by *AltaRock Energy Inc.* since 2009. The stimulation well (NWG 55-29) of the Newberry EGS system consists of a cased portion to ~1800 m depth followed by an open section to ~3000 m depth and was stimulated in 2012 by fluid-injection. In contrast to the expected MEQ distribution adjacent to the borehole along its entire open zone (Fig. 1a) – including the widely observed progressive movement to greater depths of induced seismicity with time (Fehler, 1989), – the seismicity at the Newberry Geothermal Reservoir exhibited a bimodal depth distribution of MEQs (Fig. 1b). During the seven weeks of hydraulic stimulation, a few MEQs occurred adjacent to the bottom of the open hole (within the initial 4 days) while almost no seismicity was observed in the principal stimulation zone (~1800 m to ~2500 m depth). Anomalously, 90% of the MEQs occurred above the casing shoe (at depths between 500 m and 1800 m over the next 46 days) adjacent to the cased portion of the well.

We propose that the enigmatic distribution of MEQs during the stimulation may have resulted from two alternative causes: (1) fluid injection through a leak in the casing. A segment of the casing may have been damaged in the shallow reservoir. The resulting leak would have introduced fluid overpressures and thermal stresses that could reactivate fractures. This fluid diversion in the wellbore would reduce pressures in the deep borehole (~1800 to ~3000 m depth) and staunch the potential for hydroshearing. Alternatively, (2) the shallow casing leak may have been minimal, but migration of the injected fluid from the casing shoe (~1800 m depth) to the shallow zone (~500 m to ~1800 m depth) triggered local seismic events that began after ~5 days – again as a result of elevated pore-pressures and thermal stress.

In this study, we employ both brittle failure analyses and friction experiments to explore the mechanisms behind and implications

of the observed anomalous spatial and temporal distribution of seismicity at the Newberry Geothermal Reservoir. Our results suggest that the bimodal seismicity distribution is due to leakage from the well at shallow depth. Moreover, we show that the absence of seismicity at intermediate depths cannot be explained by the observed stress and presumed stability regime but is consistent with alternate distributions of frictional strength and stability.

We begin with a description of the geological setting of the Newberry Geothermal Reservoir. Next, we provide the rationale behind and approach of various analyses that we conducted to obtain insight into the cause of the anomalous distribution of seismicity in the Newberry Geothermal Reservoir. Our analysis consists of four consecutive steps: we (i) define the controls on frictional stability within the shallow crust, (ii) define the anticipated timing of these events if driven by fluid migration, (iii) use the depth-stability analysis to show that if MEQs occur at depth, then they should also be present at all depths, and then (iv) explore reasons for the missing seismicity through inferred strain-hardening/velocity-strengthening behavior, constrained by experimental characterization. We assume constant frictional properties in efforts (i)–(iii) and test this assumption via the shear experiments (part (iv)). In addition, throughout theoretical analyses (i–iii), we adopt the in situ stresses and pore-pressures as estimated in the geological setting and treat these quantities as constants.

2. Geological setting and methods

2.1. Geological setting

The Newberry Volcano has been active for 0.5 Myr and is located in Deschutes County, Oregon, ~40 km south of Bend and ~56 km east of the crest of the Cascade Range. Well NWG 55-29 cuts through a thick flat-lying sequence of tuffs and reaches a depth of ~3 km west of the caldera rim of Newberry Volcano (Fig. 2a) (Cladouhos et al., 2011). Neither ring fractures nor faults transect the stimulated injection well (Davatzes and Hickman, 2011), eliminating the possibility of vertical conduits to transmit fluids. However, pre-existing fractures are observed in the borehole (Davatzes and Hickman, 2011). We consider a normal faulting stress regime according to the World Stress Map (Heidbach et al., 2010) and take the vertical σ_v, maximum horizontal σ_H, and minimum horizontal σ_h, stresses to be zero at the surface and use gradients of 24.1, 23.5 (N–S) and 14.9–15.8 (E–W) MPa/km, respectively with an initial hydrostatic pore-pressure P_f gradient of 8.8 MPa/km. The volcanic stratigraphy and the in situ stress regime are indicated in Fig. 2b. The average wellhead pressure during the stimulation was ~6 MPa (Cladouhos et al., 2011; Davatzes and Hickman, 2011).

2.2. Shear failure analysis

Observations such as in situ stress measurements in deep boreholes (Zoback and Healy, 1992), seismicity induced by fluid injection (Pine et al., 1983; Raleigh et al., 2013) and earthquake triggering of secondary earthquakes (Stein et al., 1992) all suggest a state of dynamic equilibrium within the upper continental crust (Townend and Zoback, 2000). Here, we explore the potential for shear failure of critically stressed fractures throughout the depth of the geothermal reservoir. We use the Mohr–Coulomb failure criterion (Fig. 3) to define the shear strength, τ_s, for brittle failure of pre-existing fractures:

$$\tau_s = C_0 + \mu_s \cdot \sigma_{neff} = C_0 \mu_s \cdot (\sigma_{tot} - \alpha_b \cdot P_f) \quad (1)$$

where C_0 is cohesion; μ_s is the coefficient of friction (tangent of friction angle φ); σ_{neff} is the effective normal stress; σ_{tot} is the total normal stress; and α_b is the Biot coefficient.

The pre-existing fractures are considered to be optimally oriented for shear failure with the fracture normal at an angle θ to the maximum principal stress σ_1 (Fig. 3).

Thus, we have:

$$\sigma_{neff} = \frac{\sigma_1' + \sigma_3'}{2} + \frac{\sigma_1' - \sigma_3'}{2} \cos 2\theta \quad (2)$$

$$\tau = -\frac{\sigma_1' - \sigma_3'}{2} \sin 2\theta \quad (3)$$

where τ is the critical shear stress; σ_1' and σ_3' are the effective maximum and minimum principal stresses, respectively; and 2θ is equal to $\varphi+\pi/2$. In this study, σ_1 and σ_3 denote the vertical and minimum horizontal stresses, respectively. Combining Eqs. (1) and (3), yields:

$$\frac{\sigma_1'}{\sigma_3'} = \frac{(\mu_s^2+1)^{1/2} + \mu_s + 2C/\sigma_3'}{(\mu_s^2+1)^{1/2} + \mu_s} \quad (4)$$

Extending the principal stress as a function of in situ stress gradients, reservoir depth, initial hydrostatic pore-pressure, and applied wellhead pressure, we can rewrite Eq. (4) as follows:

$$F_{pot} = \frac{\sigma'(T)}{\sigma} = \frac{(\gamma_1 - \alpha_b \cdot \gamma_f) \cdot z - \alpha_b \cdot \Delta P_w}{(\gamma_3 - \alpha_b \cdot \gamma_f) \cdot z - \alpha_b \cdot \Delta P_w} \quad (5)$$

$$F_{crt} = \frac{(\mu_s^2+1)^{1/2} + \mu_s + 2C/\sigma_3'}{(\mu_s^2+1)^{1/2} - \mu_s} = \frac{(\mu_s^2+1)^{1/2} + \mu_s + 2C/[(\gamma_3 - \alpha_b \cdot \gamma_f) \cdot z - \alpha_b \cdot \Delta P_w]}{(\mu_s^2+1)^{1/2} - \mu_s} \quad (6)$$

where γ_1, γ_3, and γ_f, represent the gradients of σ_1, σ_3, and P_f, respectively; z is the reservoir depth and ΔP_w is the local wellhead pressure (Fig. 3). We define Eq. (5) as the shear failure potential F_{pot} and Eq. (6) as the critical failure index F_{crt} to determine whether a critically stressed fracture would fail at a given reservoir depth. If the cohesion C_0 is null, then the critical failure index F_{crt} is controlled only by the coefficient of friction of the pre-existing fractures.

Before stimulation, F_{pot} is a constant value defined by the initial in situ pore-pressure and in situ stresses. During fluid injection, F_{pot} becomes a function of both depth and the fluid pressure. More realistically, injecting cold fluid in the hot reservoir induces thermal contraction of the rock, reducing the effective stresses acting on the fracture. The upper-bound for the induced thermal stress is approximated as:

$$\sigma_{thermal} = \alpha \cdot \Delta T \cdot E \quad (7)$$

where α is the linear thermal coefficient; ΔT is temperature change; E is the Young's modulus of the reservoir rocks and a full displacement constraint is assumed. This yields the shear failure potential:

$$F_{pot} = \frac{(\gamma_1 - \alpha_b \cdot \gamma_f) \cdot z - \alpha_b \cdot \Delta P_w - \sigma_{thermal}}{(\gamma_3 - \alpha_b \cdot \gamma_f) \cdot z - \alpha_b \cdot \Delta P_w - \sigma_{thermal}} \quad (8)$$

Thus the relation between F_{pot} and F_{crt} with respect to the shear failure events in the geothermal reservoir can be described as: (1) If F_{pot} is equal to or greater than F_{crt}, then shear failure may occur. (2) If F_{pot} is less than F_{crt}, then no failure occurs.

For the scenario of a casing leak in the shallow reservoir, we assume that the wellhead pressure in the leaking window is transmitted to the open zone. Thus, we use this method to examine the shear failure potential on pre-existing fractures exposed to the same ΔP_w.

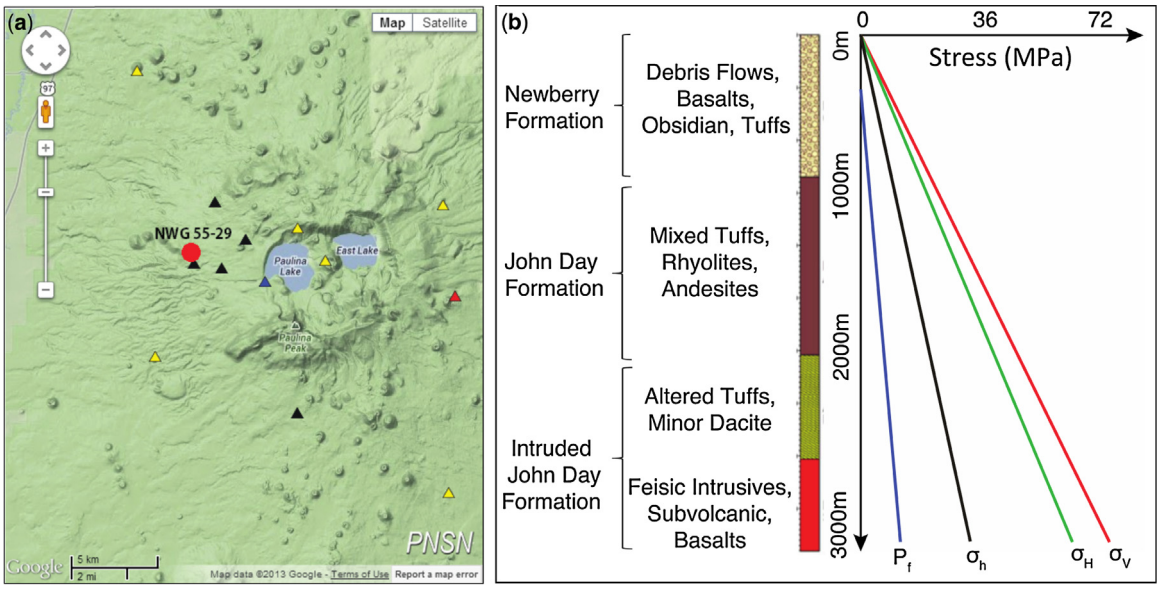

Fig. 2. (a) Location of well NWG 55-29 (from Google Earth). (b) Stratigraphy and stress regime of well NWG 55-29.

2.3. Pore-pressure diffusion analysis

In well injection scenarios, pore-pressure diffusion is an important factor that may influence the timing of seismicity (Evans et al., 2005; Lee and Wolf, 1998; Shapiro et al., 1997). In the low-frequency limit of Biot's (1962) equations, the pore-pressure diffusion from a borehole in a fluid-saturated porous medium is expressed as (Biot, 1956; Shapiro et al., 2002):

$$\beta\phi\frac{\partial p}{\partial t} = \frac{\partial}{\partial t}\left[\frac{k}{\eta}\cdot r^2\cdot\left(\frac{\partial p}{\partial r}\right)\right] \tag{9}$$

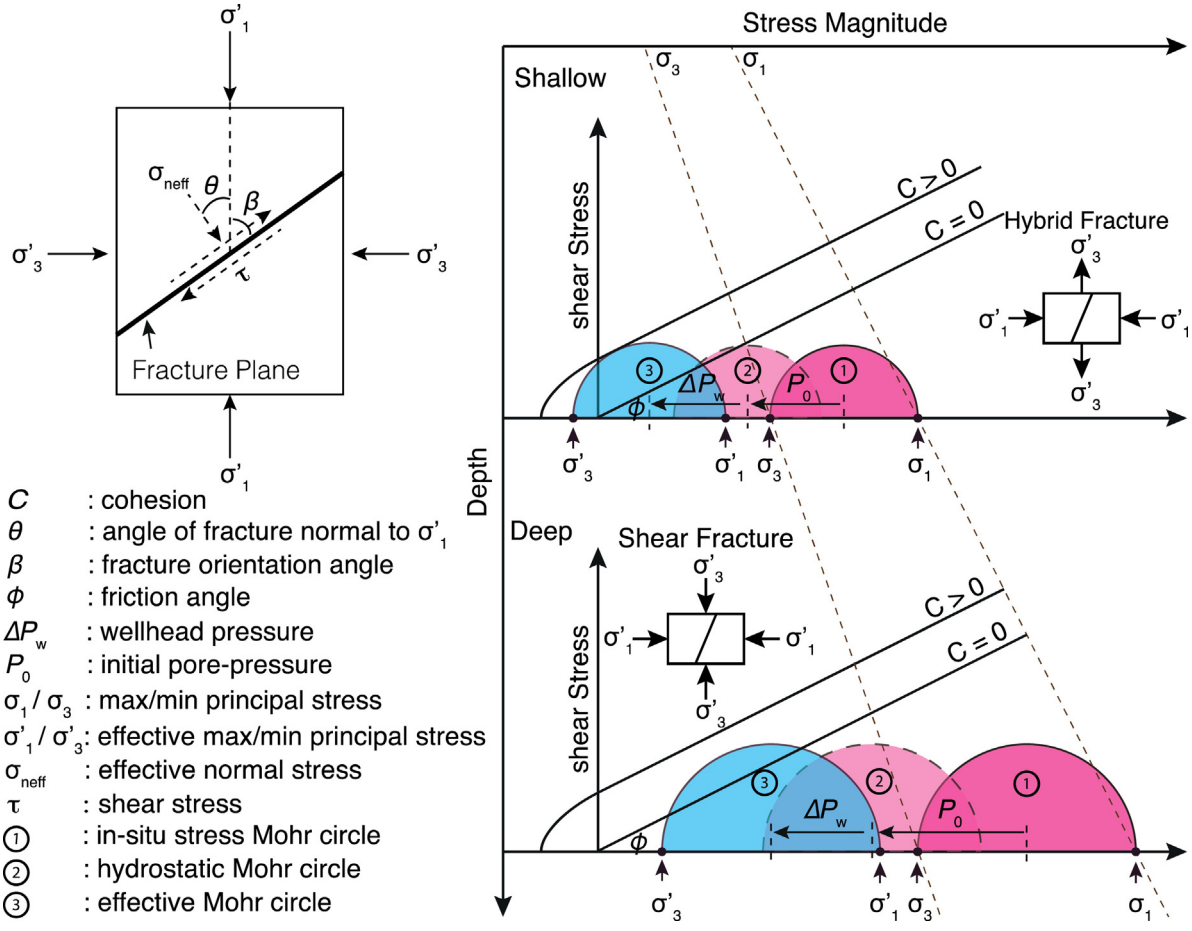

Fig. 3. Schematic fracture plane with respect to stress configuration (left side) and depth and fluid pressure dependent Mohr circles (right side).

where β is the compressibility coefficient; Φ is the porosity; p is the pressure; t is the diffusion time; r is the diffusion length; η is the viscosity of the fluid; k is the permeability. The solution to Eq. (9) for a Heaviside pressure pulse applied at the origin (Shapiro et al., 1997) suggest that the distance from the injection point to the triggering front can be described as:

$$r^2 = 4\pi Dt = 4\pi t \frac{N\kappa}{\eta} \tag{10}$$

where D is the hydraulic diffusivity and N is a poroelastic modulus defined as follows (Delépine et al., 2004; Lachenbruch, 1980; Shapiro et al., 1997):

$$N = \left[\frac{\phi}{K_f} + \frac{\alpha}{K_g}\right]^{-1} \tag{11}$$

where $\alpha = 1 - K_d/K_g$; K_d is the drained bulk modulus of the dry frame; K_g is the bulk modulus of the grains; and K_f is the bulk modulus of the fluid.

We use Eq. (10) to estimate the time necessary for injected fluid to diffuse from the top of the open hole (base of the casing) to the shallow reservoir and test whether this can explain the observed timing of anomalous seismicity at shallow depths in the reservoir. We assume spherical pore-pressure diffusion in a homogeneous medium, and we focus on upward diffusion along a vertical path as this is the shortest distance to reach the shallow reservoir and thus defines the shortest critical diffusion time t_c.

2.4. Friction experiments

In the foregoing analyses, we have assumed constant frictional properties of the geothermal reservoir rocks. However, in reality, the frictional characteristics are expected to depend on factors such as rock composition and the depth-dependent in situ pressure and temperature conditions (Den Hartog and Spiers, 2013). Hence, we performed friction experiments to determine the frictional properties of pre-existing fractures as a function of depth and as such provide insight into the mechanisms of the anomalous distribution of seismicity.

2.4.1. Sample material and experimental procedure

We collected 5 samples from drilling cuttings from well NWG 55-29 for friction experiments. Samples 1 and 2 were collected from the shallow reservoir where abundant MEQs occurred, while samples 3 to 5 were taken from the missing seismic zone at depths between ~1800 m and ~3000 m. After cleaning the samples to remove the drilling mud and possible drill bit fragments, the samples were crushed and powdered in a disk mill, and finally sieved to a particle size less than 150 μm. The mineralogical composition of the samples was characterized via X-Ray Diffraction analysis (XRD), which shows that the samples were dominated by three groups of minerals: carbonate (mainly calcite), phyllosilicates and tectosilicates (Table 1).

The experiments were performed with a biaxial testing apparatus (Fig. 4a), using the same set-up and following similar procedures as (Samuelson et al., 2008). In this machine, two gouge layers are sandwiched between three roughened steel forcing blocks with a contact area of 50 mm × 50 mm. We performed experiments at room temperature on water-saturated gouge layers with an initial thickness of 5 mm. To ensure that gouge layers were flat and identical in each experiment, they were constructed using a leveling jig and a measured mass (Frye and Marone, 2002).

Shear loading was attained by forcing the central block down at a constant velocity of 10 μm/s, while applying a normal load of 15 MPa perpendicular to the shear direction. After the

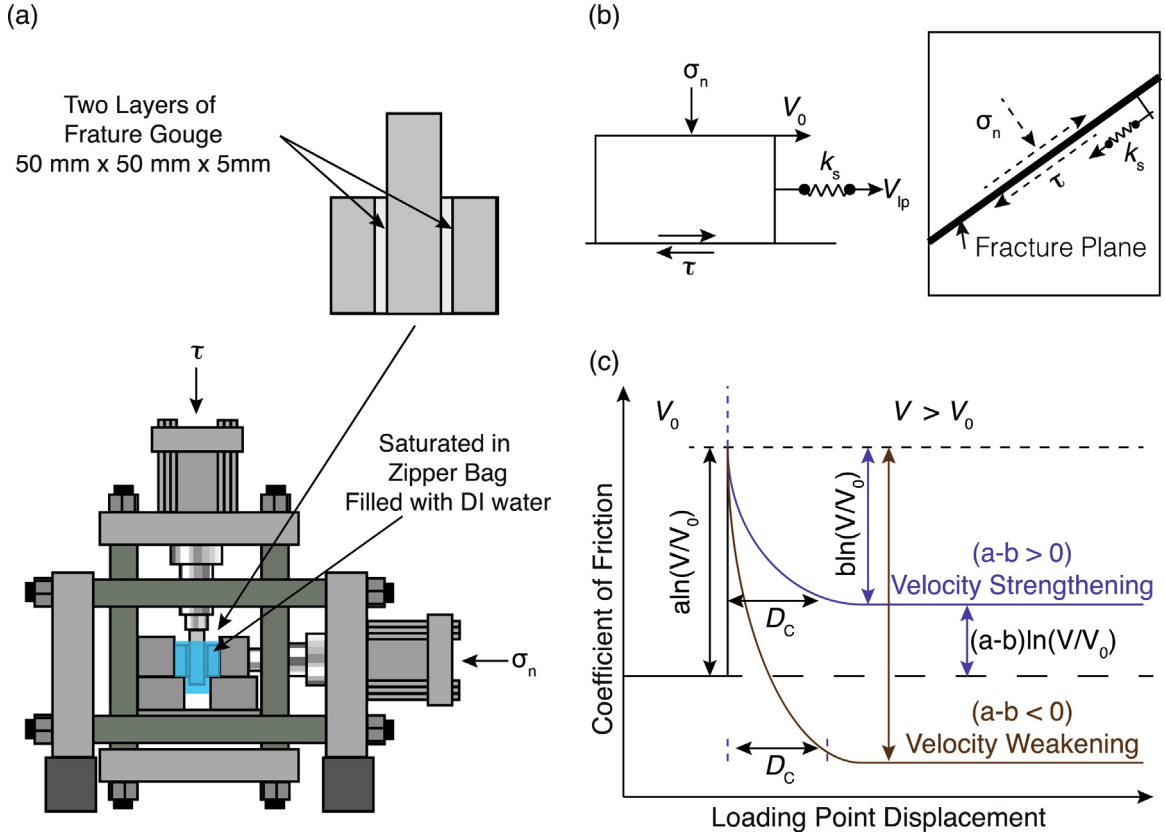

Fig. 4. (a) Double-direct shear geometry in a biaxial load frame. (b) Conceptual sliding model representing the fracture/fault sliding behavior. (c) Idealized RSF friction response to an increased velocity step showing two alternative frictional behaviors: velocity strengthening and velocity weakening.

Table 1
Information of drilling core samples from stimulation well NWG 55-29.

No.	Depth (m)	Formation	Mineral Compositions
S1	~701	Newberry	81% Albite, 17% clinopyroxene, 2% hematite
S2	~1407	John Day	49% Andesine, 14% calcite, 13% montmorillorite, 11% clinochlore, 7% quartz, 3% vermiculite
S3	~2139	Intruded John Day	60% Albite, 20% quartz, 14.8% clinochlore, 3.5% calcite, 2.6% muscovite
S4	~2603	Intruded John Day	70% Albite, 12% quartz, 11% phlogopite, 2.5% chlorite, 2.1% stilbite, 0.5% calcite, 1.9% others
S5	~2904	Intruded John Day	56.4% Albite, 23.6% quartz, 14.6% orthoclase, 4.4% clinochlore, 0.6% muscovite, 0.4% calcite

achievement of steady-state friction, the sliding velocity was stepped in the range from 1 μm/s to 300 μm/s until a displacement of 9 mm was reached. The normal stress was next raised to 45 MPa and the velocity sequence was repeated, reaching a final displacement of 18–20 mm. The effect of calcite on the frictional properties of the Newberry samples was tested by performing additional experiments on samples 2 and 4 after leaching with 12% hydrochloric acid to remove the calcite.

2.5. Data analysis

We calculated the coefficient of friction μ as a function of shear displacement for our experiments using $\mu = \tau/\sigma_n$. The velocity dependence of friction was interpreted in the framework of the rate and state friction (RSF) theory (Fig. 4b) (Dieterich, 1979, 1978; Ruina, 1983). In the RSF approach to modeling fracture slip, the friction coefficient is written as (Dieterich, 1978; Marone, 1997; Scholz, 1998):

$$\mu = \mu_0 + a \ln\left(\frac{V}{V_0}\right) + b \ln\left(\frac{V_0\theta}{D_c}\right) \quad (12)$$

$$\frac{d\theta}{dt} = 1 - \frac{V\theta}{D_c} \quad (13)$$

where μ_0 is the coefficient of friction at a reference velocity V_0; θ is a state variable, a and b are friction parameters which represent, respectively, the effect of instantaneous and displacement-dependent changes in friction from V_0 to $V = eV_0$; and D_c is the critical slip distance over which evolution to a new steady state takes place. Frictional slip instability is determined in part by the parameter $(a-b)$ derived from Eq. (12) for a finite step in velocity, yielding (Dieterich, 1979; Ruina, 1983; Scholz, 1998):

$$a - b = \frac{\Delta v_{ss}}{\Delta \ln V} \quad (14)$$

A positive value of $(a-b)$ denotes velocity-strengthening behavior indicative of stable, aseismic slip (Gu et al., 1984), while a negative $a-b$ indicates velocity-weakening behavior, which is potentially unstable (Fig. 4c). The RSF friction parameters were determined from our experiments by solving Eqs. (12) and (13), coupled with an equation describing elastic interaction with the testing machine, using the fitting method described by Marone (1998) and Blanpied et al. (1998).

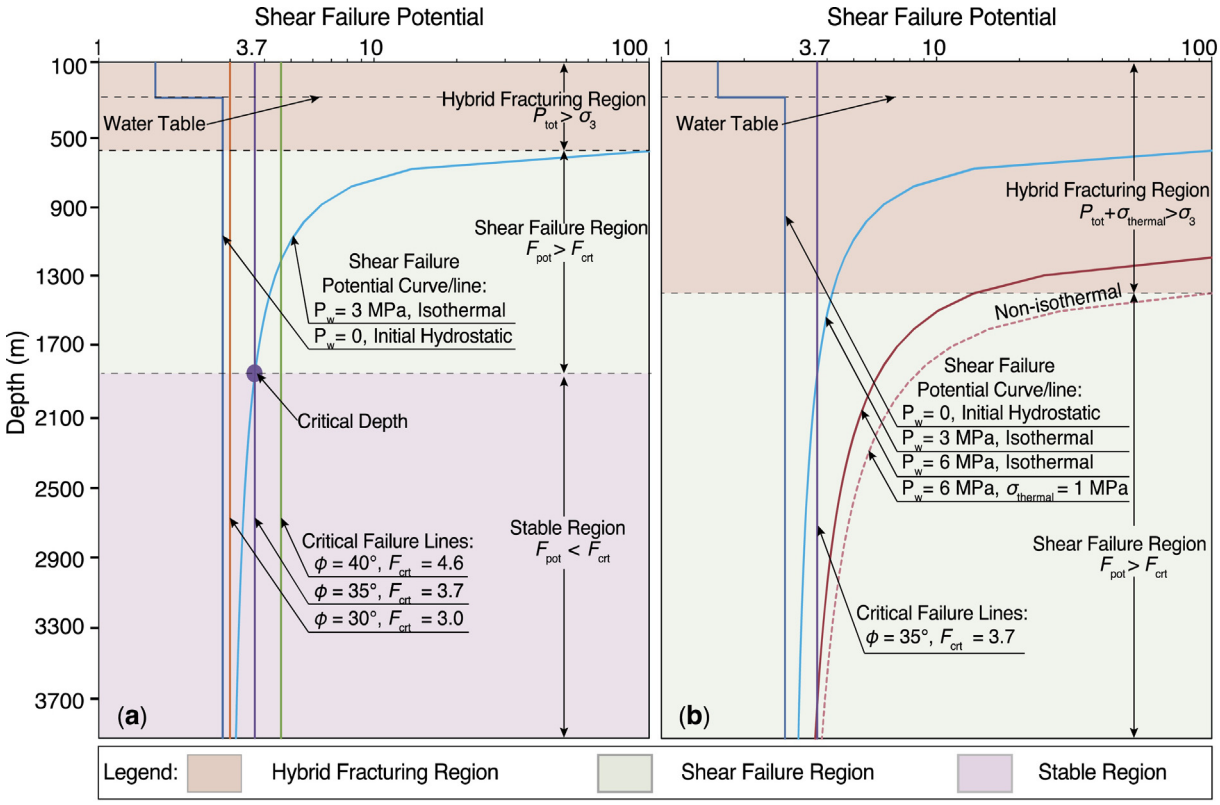

Fig. 5. Shear failure potential and critical failure as a function of depth for wellhead pressure applied at all depth. (a) Effect of coefficient of friction of pre-existing fractures. Assuming the friction angle is 35°, the value of shear failure potential (blue curve) is greater than that of the critical failure line (purple line) above the critical depth at ~1900 m, while it is smaller below this depth. If the fracture has a larger (or smaller) friction angle than 35° (or 30°), the stability region will increase (or decrease). (b) Effects of magnitude of wellhead pressure and thermal stress. When wellhead pressure increases from 3 MPa to 6 MPa, the shear failure region will be enlarged with depth. Thermal stress will enhance the instability along the depth. (For interpretation of the references to color in this figure legend, the reader is referred to the web version of this article.)

Frictional stability depends on the critical stiffness K_c defined as:

$$K_c = \frac{\sigma_n(b-a)}{D_c} \tag{15}$$

As shown by Gu et al. (1984), instability may occur if the loading stiffness K is smaller than the effective-rheologic stiffness K_c.

If we assume a circular dislocation (fracture) in a homogeneous medium, the effective shear stiffness around a fracture of diameter L is (Chinnery, 1969; Scholz, 2002; Starr, 1928):

$$K = \eta \cdot \frac{G_s}{L} \tag{16}$$

where η is a geometric factor and G_s is the shear modulus. Assuming the crack in the reservoir is penny-shaped, η has the value of $7\pi/24$. Combing Eq. (15) and (16), we find that the critical fracture length L_c for instability is:

$$L_c = \eta \cdot \frac{G_s \cdot D_c}{\sigma_n \cdot (b-a)} \tag{17}$$

For fractures smaller than L_c, (i.e., $K > K_c$) stable sliding will occur, while for those larger than L_c (i.e., $K < K_c$), unstable slip can result.

3. Results

3.1. Shear failure analysis

Failure may be induced on critically oriented fractures in the reservoir by the application of sufficient wellhead pressure. Fig. 5a shows that when the friction angle of fractures is 30° and the wellhead pressure is 3 MPa, the F_{pot} at each depth is larger than that of F_{crt}, implying that all the critically stressed fractures will fail to slip at all depths. If fractures are frictionally stronger, the F_{crt} in the deeper reservoir will be larger than F_{pot}, resulting in a stable region in the deep reservoir, but rendering the shallow reservoir unstable ($F_{pot} > F_{crt}$). Increasing wellhead pressure (e.g., from 3 MPa to 6 MPa) can both enlarge the regions of hybrid fracturing (shear failure and tensile failure) and hydroshearing where $F_{pot} > F_{crt}$ (Fig. 5b). In addition, when thermal stresses are considered at each depth (quenching), the zones of instability spread.

3.2. Pore-pressure diffusion

We consider a possible migration of fluids from the deep open zone (top of the open zone at ~2000 m) to the shallow seismic zone and calculate pressure-diffusion under two end-member permeability scenarios: (1) migration through high permeability fractures (k = 10 mD) and (2) migration through low permeability matrix (k = 10 μD). During the stimulation, injection of water was completed in three cycles: about 7 days for the first cycle, then 7 days for the second cycle and 14 days for the third cycle after a hiatus of 7 days (Fig. 6a). The depths of seismic events with time are indicated in Fig. 6b. The timing of these seismic events indicates an appropriate synchronous response to the injected wellhead pressure. The rate of pore-pressure diffusion in the fractures and rock matrix shows a significant difference that in the first injection cycle, the vertical distances from the depths of all seismic events to the reference depth are larger the pore-pressure diffusion length through the matrix.

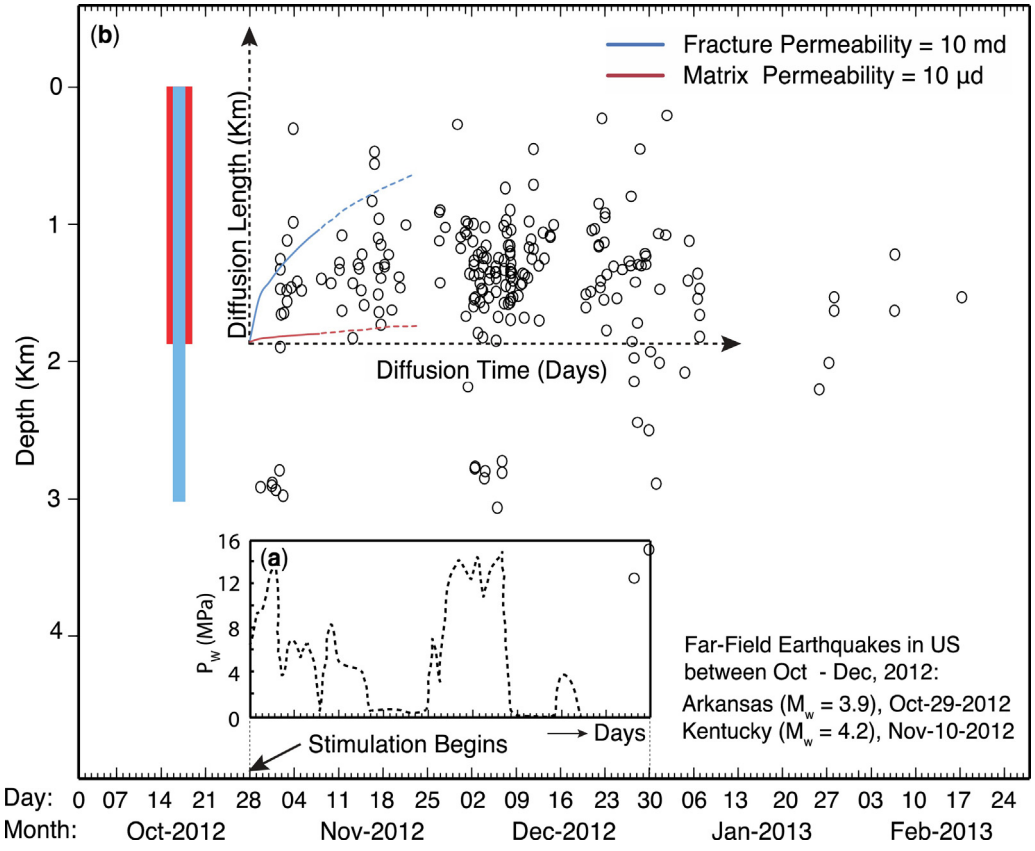

Fig. 6. (a) Injection wellhead pressure with time. (b) Pore-pressure diffusion length with time compared with elevations of seismic events with time. The vertical distances between the top of uncased wellbore portion and some seismic events in shallow reservoir (above 1000 m) are beyond the maximum diffusion front when reservoir permeability is 10 md.

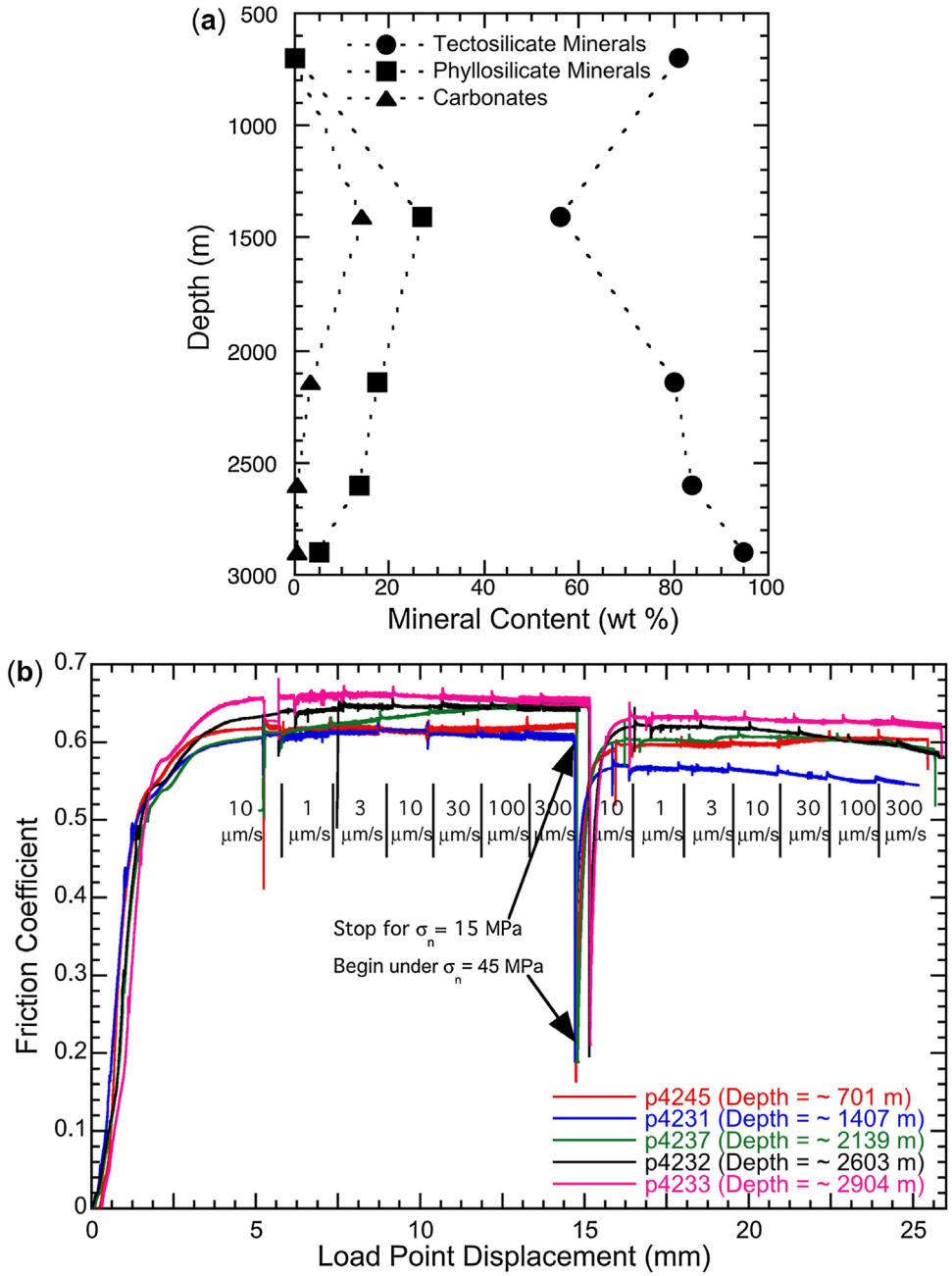

Fig. 7. (a) Mineral contents with depths. (b) Friction-load point displacement curves of examined samples under normal stresses of 15 MPa and 45 MPa, respectively.

3.3. *Friction experiments*

A preliminary appraisal of the observed seismicity by both lithostatic (Section 3.1) and distributed parameter models (Section 3.2) suggests that if shear failure occurred in the deep reservoir (~3000 m) it should also occur in the upper open zone. Thus the observed bimodal distribution of seismicity cannot be fully explained by a model with uniform frictional properties with depth. Therefore, we determined the frictional slip stability as a function of depth from our shear experiments to clarify the distribution of MEQs.

The composition of the samples used for the experiments is plotted versus depth in Fig. 7a. All samples are dominated by tectosilicates with lesser amounts of phyllosilicates and calcite. The phyllosilicates and calcite contents reach a maximum at a depth of ~1500 m while the amount of tectosilicates is lowest at this depth. The friction curves of all shear experiments were similar (Fig. 7b). The friction coefficient measured at the end of each constant normal stress portion (i.e. at displacements of 9 and 18 mm for 15 and 45 MPa, respectively) are plotted in Fig. 8 versus depth, while $(a-b)$ values at 15 and 45 MPa normal stress are shown versus depth in Figs. 9 and 10.

The measured $(a-b)$ values of samples are predominantly positive (velocity strengthening) at the conditions of our experiments. At shallow depth (~700 m) and at the base of the open zone (~2900 m), the $(a-b)$ magnitudes are near zero or close to velocity neural, while at ~1400 m, $(a-b)$ is more positive, representing more velocity strengthening behavior. The $(a-b)$ values of samples with/without calcite at 15 MPa and 45 MPa normal stress are shown in Fig. 11.

The results show similar trends of composition of samples and friction properties with depth, suggesting a possible mineralogical

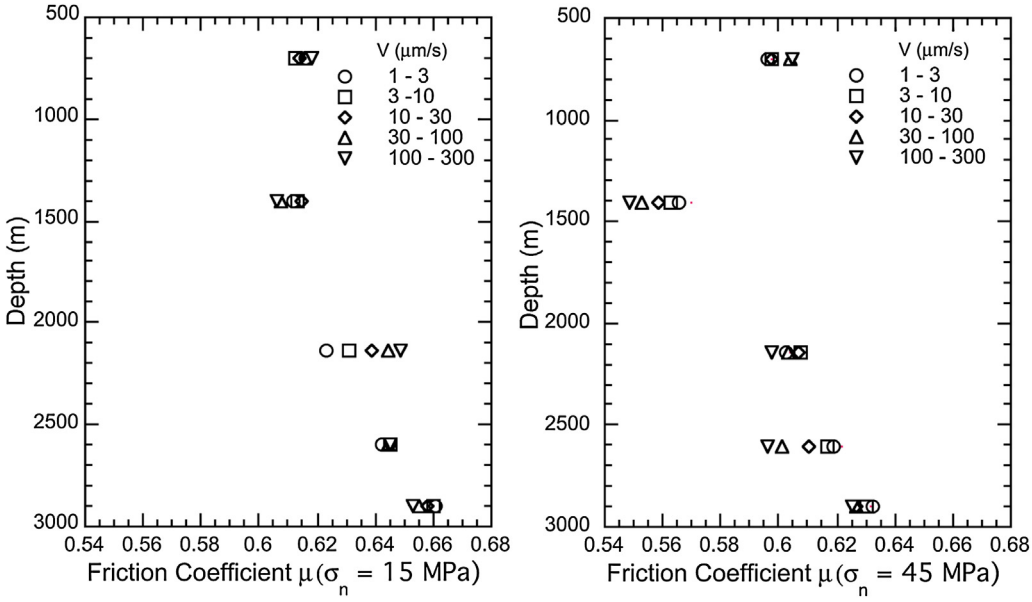

Fig. 8. Steady sliding friction μ of examined samples with depths before each velocity step under normal stresses of 15 MPa and 45 MPa, respectively.

control on the MEQs at intermediate depth. The critical friction slip distance increases with post-step velocity (Fig. 12a). We used the modeled RSF parameters along with a bulk modulus of 17 GPa and Poisson ratio of 0.27 (Izadi and Elsworth, 2013; Li et al., 2012) to estimate the critical fracture radius L_c for frictional instability and earthquake nucleation. The fracture length increases with increasing sliding velocity (Fig. 12b). Our data suggest a minimum fracture radius of ~7 m.

4. Discussion

Considering the first possible cause that the casing leak in the shallow reservoir may contribute to the bimodal distribution of the MEQs, shear failure analysis indicates that the newly introduced fluid penetrating the shallow reservoir (above ~1800 m) due to casing leak will enhance local instability of fractures and induce MEQs. The less critically oriented fractures in the shallow reservoir could also be reactivated due to the higher shear potential F_{pot} compared to that of the deep reservoir (~3000 m), resulting in more seismic events. Meanwhile, wellhead pressure ΔP_w in the open zone (below ~2000 m) will decrease due to the shallow casing leak. As a result, the residual ΔP_w in the open zone may not be sufficient to continue reactivating local pre-existing fractures, which explains why the MEQs diminish in the deep zone (~3000 m).

For the second possible cause, pore-pressure diffusion analysis demonstrates that, for reservoir fractures with a permeability of 10 mD, the estimated fluid migration time does not match the timing of the observed shallow MEQs within the initial 4 days of stimulation. Furthermore, the previous logging and testing of well NWG 55-29 suggests that the pre-existing fractures lack significant permeability (estimated at ~10 μD in impermeable zone

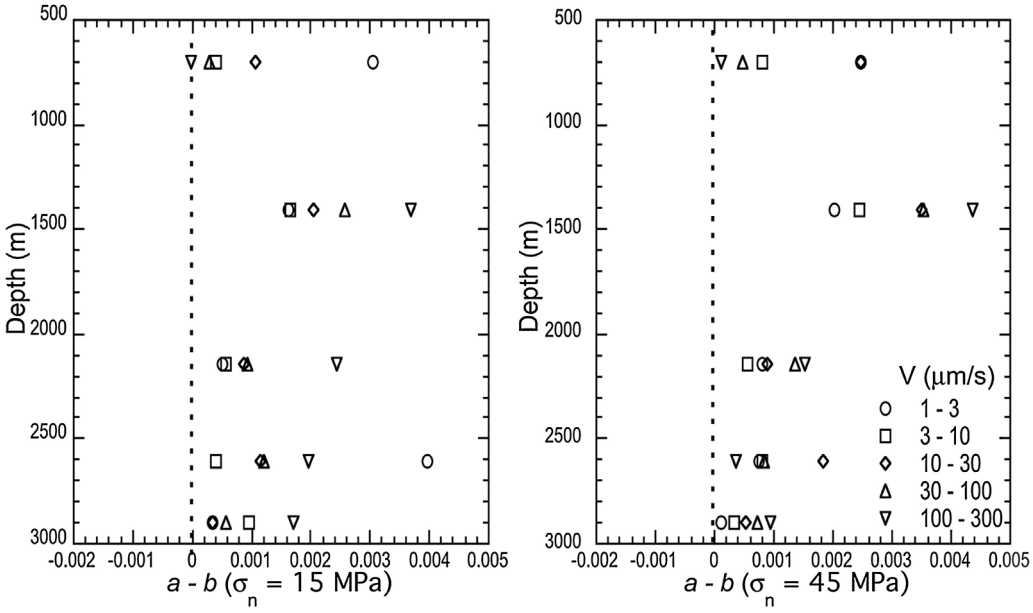

Fig. 9. Friction parameter $(a-b)$ of examined samples with depths for each velocity step under normal stresses of 15 MPa and 45 MPa, respectively.

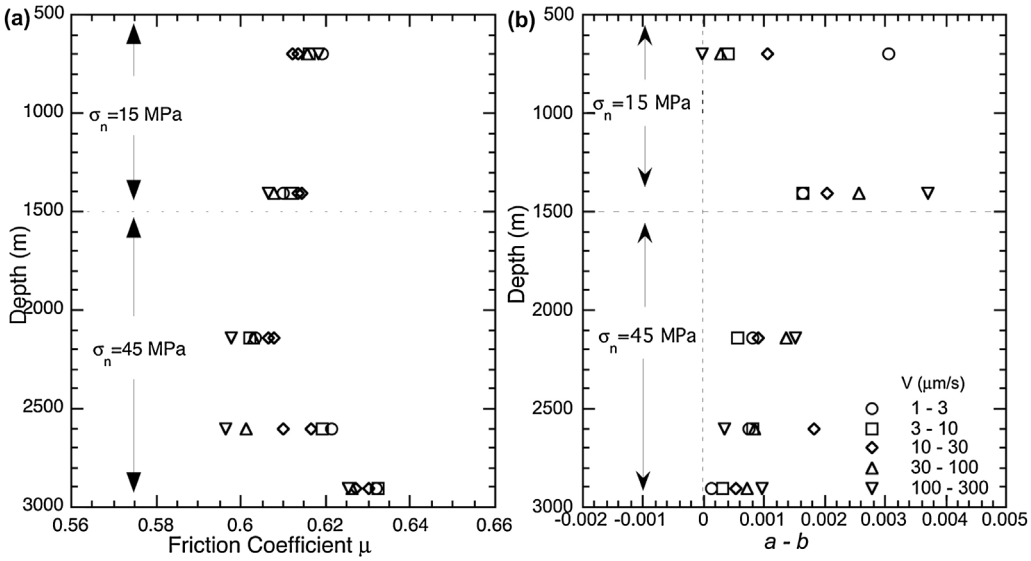

Fig. 10. (a) Friction coefficient μ and (b) parameter $(a-b)$ with depths of approximate in situ normal stress.

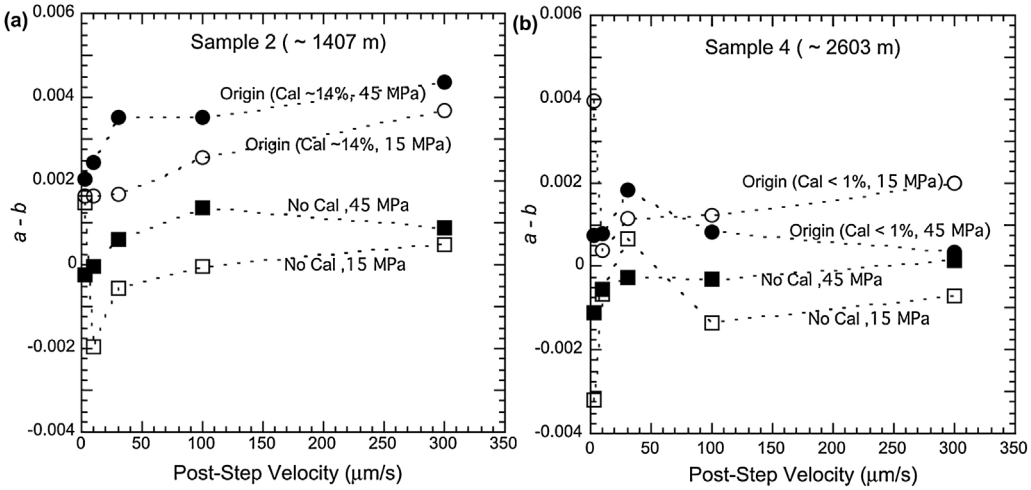

Fig. 11. Comparison of frictional parameter $(a-b)$ between calcite contained and calcite removed samples 2 and 4.

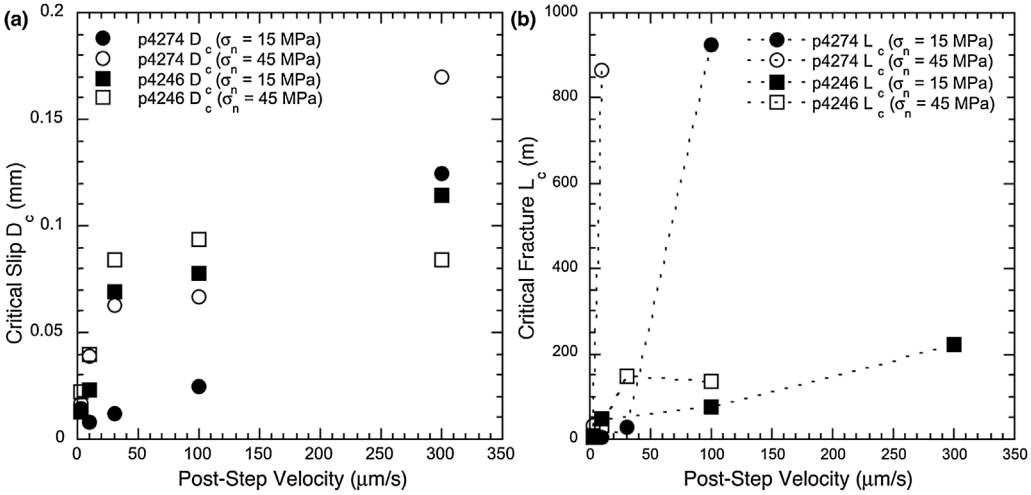

Fig. 12. (a) Critical slip distance and (b) critical fracture length with increasing velocity.

and ~3.25 mD in permeable zone) (Petty et al., 2013; Spada et al., 2013). Hence, a realistic diffusion length should be considerably shorter than the upper-limit end-member scenario and it is plausible that the water cannot migrate upwards and generate critical overpressures sufficiently quickly. As a result, the unmatched timing between MEQs and fluid migration (Fig. 6) implies that the deep injected fluid is unlikely to be the major cause of early shallow seismic events.

Based on our friction experiments, and previous studies, we consider four factors that may be important to explain the missing seismicity at intermediate depths: viz. contrasting mineral compositions, pore-pressures, temperatures and fracture sizes at the sampled depths in the reservoir. In terms of mineralogy, frictional strength μ shows the opposite trend compared to parameter $(a-b)$ with depth. The phyllosilicate-rich materials exhibit low frictional strength and velocity-strengthening behavior while tectosilicate-rich materials show high frictional strength with velocity-neutral (or minimum velocity-weakening behavior) (Figs. 7a and 10) suggesting that $(a-b)$ and μ are strongly mineral group dependent. This relation is also observed in previous studies (Ikari et al., 2011; Kohli and Zoback, 2013; Niemeijer and Collettini, 2013). The comparison of $(a-b)$ values between samples with calcite and those in which the calcite was removed shows that dissolving the calcite decreases $(a-b)$ at room temperature (Figure 11), implying that the dissolution of calcite can decrease frictional stability. Because wet calcite-rich fault gouge exhibits stable slip below 80–100 °C, unstable slip at 10–550 °C, and is stable again at 590 °C (Verberne et al., 2014), $(a-b)$ values of samples at in situ temperatures (100–250 °C) are expected to be lower than the values measured in the current experiments conducted at room temperature. However, the effects of calcite on $(a-b)$ values are expected to be minimal in the deep reservoir where the calcite content is negligible. This is supported by our result showing similar $(a-b)$ values for sample with and without (~0.5%) calcite.

Pore pressure is another important factor that may influence frictional slip stability (Scholz, 1998). In our experiments, we observed that the $(a-b)$ values of samples from the shallow reservoir are slightly lower when deformed at a normal stress of 15 MPa as opposed to 45 MPa. Samples from the deep reservoir, on the other hand, show slightly higher values at 15 MPa than at 45 MPa. Although the differences are small, they suggest that a reduction of the effective normal stress brought about by an increase in the pore pressure due to plausible casing leak in the shallow reservoir may result in a lower local $(a-b)$ value, while increasing the pore pressure due to fluid injection in the deep reservoir can increase the local $(a-b)$ value.

In summary, from the above we infer that the in situ frictional slip stability of the shallow reservoir could have been less than implied by our measured $(a-b)$ data, because: (1) the temperature of the calcite-rich shallow reservoir (~1400 m) is about 100 °C and previous studies suggest that $(a-b)$ values are lower at this higher temperature; (2) An abrupt increase in fluid pressure as a result of casing leak in this calcite-rich region also decreases frictional stability and (3) low temperature leaking fluid dissolves the calcite, resulting in a further reduction of $(a-b)$. In addition, $(a-b)$ values at these depths are very small and close to velocity neutral. Thus the perturbation by the increased pore-pressure as well as the temperature effect may result in a shift of local $a-b$ magnitudes from positive to negative.

In the zone where seismic events are absent, the calcite content of samples decreases with depth and is negligible at the base of the open zone. Thus the measured positive $(a-b)$ values in the deep reservoir may be slightly influenced by the temperature that promotes velocity-weakening behavior in calcite (i.e., $(a-b)$ values may be slightly lower than the measured ones). However, this slight effect is offset by the pore-pressure perturbation that increasing local fluid pressure (or decreasing effective normal stress) at greater depths will have, thereby increasing local $a-b$ values (i.e., local frictional stability is enhanced). As a result, the measured positive $a-b$ values may be close to the in situ values, implying that only aseismic events could occur in the deep zone. Furthermore, the migration of cold injected fluid through the fractures could remove the retrograde-soluble calcite and may gradually decrease the $(a-b)$ values. In this manner the initial velocity strengthening properties of preexisting fractures could be transformed to velocity weakening, with the potential for frictional instability.

In addition to mineralogical influences on stability, the distribution of fracture sizes is an important factor to determine the potential for instability when $(a-b)$ values are negative. Our results suggest that only fractures with negative $(a-b)$ values and lengths (radius) greater than ~7 m may slip unstably. However, fractures with length less than 7 m are conditionally stable. If in situ fault creep velocities are slower than the experimental sliding velocity, the real critical fracture length could be smaller than the lowest fracture length derived from our data. Based on this analysis, we can speculate that, if the $(a-b)$ values of the preexisting fractures were initially negative, then fracture lengths in the stable aseismic zone must be smaller than this threshold of ~7 m. This speculation needs to be validated by further in situ reservoir fracture characterization.

5. Conclusion

Differing from other expected distribution patterns of induced MEQs with depth, this bimodal depth distribution of MEQs at the Newberry Geothermal Reservoir suggests unusual controls by fluid permeation and reservoir mineralogy and state. Our analyses introduce the following conclusions: (1) the unusual and unexpected penetration of excess fluid pressures in the shallow zone is plausible mainly due to the casing leak in the shallow reservoir. This result is further confirmed by the second observation that indeed the casing is damaged at shallow depth (~700 m). (2) The diminished seismicity in the deep open zone is plausibly associated by fluid loss (wellhead pressure drop) as a result of the shallow leak. (3) An upward-migrating fluid pressure pulse is incapable of inducing seismicity in the shallow reservoir (above ~1000 m), but may partially contribute to the occurrence of seismicity near the top of casing shoe (~1800 m). (4) The observation of missing seismic events between ~1800 m and ~2500 m during the stimulation plausibly results from slight velocity strengthening properties in the reservoir and in particular on local preexisting fractures. Aseismic events may still occur in this intermediate zone, in the form of slow sliding slip or creep events, but may be below the threshold observed by the seismic monitoring.

Acknowledgements

This work is the result of partial support provided by DOE Grant DE-EE002761 and NSF grants EAR1045825 and EAR1215856. This support is gratefully acknowledged.

Appendix A. Supplementary data

Supplementary data associated with this article can be found, in the online version, at doi:10.1016/j.geothermics.2015.04.005

References

Bachmann, C.E., Wiemer, S., Woessner, J., Hainzl, S., 2011. Statistical analysis of the induced Basel 2006 earthquake sequence: introducing a probability-based monitoring approach for enhanced geothermal systems. Geophys. J. Int. 186, 793–807, http://dx.doi.org/10.1111/j.1365-246X.2011.05068.x

Biot, M.A., 1956. Theory of propagation of elastic waves in a fluid-saturated porous solid. II. Higher frequency range. J. Acoust. Soc. Am., http://dx.doi.org/10.1121/1.1908241

Biot, M.A., 1962. Mechanics of deformation and acoustic propagation in porous media. J. Appl. Phys. 33 (4), 1482–1498.

Blanpied, M.L., Marone, C.J., Lockner, D.A., Byerlee, J.D., King, D.P., 1998. Quantitative measure of the variation in fault rheology due to fluid–rock interactions. J. Geophys. Res. Solid Earth 103, 9691–9712, http://dx.doi.org/10.1029/98JB00162

Chinnery, M.A., 1969. Theoretical fault models. In: Kasahar, K., Stevens, A.E. (Eds.), A symposium on Processes in the Focal Region, vol. 37. Publ. Dom. Obs., Ottawa, pp. 211–223.

Cladouhos, T.T., Petty, S., Callahan, O., Osborn, W., Hickman, S., Davatzes, N.,2011. The role of stress modeling in stimulation planning at the Newberry Volcano EGS Demonstration Project. In: Thirty Sixth Workshop on Geothermal Reservoir Engineering. Stanford University, Stanford, CA, p. 8.

Davatzes, N.C., Hickman, S.H., 2011. Preliminary Analysis of Stress in the Newberry EGS Well NWG., pp. 29–55.

Delépine, N., Cuenot, N., Rothert, E., Parotidis, M., Rentsch, S., Shapiro, S.A., 2004. Characterization of fluid transport properties of the Hot Dry Rock reservoir Soultz-2000 using induced microseismicity. J. Geophys. Eng., http://dx.doi.org/10.1088/1742-2132/1/1/010

Den Hartog, S., Spiers, C.J., 2013. Influence of subduction zone conditions and gouge composition on frictional slip stability of megathrust faults. Tectonophysics 600, 75–90, http://dx.doi.org/10.1016/j.tecto.2012.11.006

Dieterich, J.H., 1978. Time-dependent friction and the mechanics of stick-slip. Pure Appl. Geophys. PAGEOPH 116, 790–806, http://dx.doi.org/10.1007/BF00876539

Dieterich, J.H., 1979. Modeling of rock friction. 1. Experimental results and constitutive equations. J. Geophys. Res. Solid Earth, 2161–2168, http://dx.doi.org/10.1029/JB084iB05p02161

Elsworth, D., Goodman, R.E., 1986. Characterization of rock fissure hydraulic conductivity using idealized wall roughness profiles. Int. J. Rock Mech. Min. Sci. Geomech. Abstr. 23, 233–243, http://dx.doi.org/10.1016/0148-9062(86)90969-1

Evans, K.F., Genter, A., Sausse, J., 2005. Permeability creation and damage due to massive fluid injections into granite at 3.5 km at Soultz. 1. Borehole observations. J. Geophys. Res. Earth, 110, http://dx.doi.org/10.1029/2004jb003168

Fehler, M.C., 1989. Stress control of seismicity patterns observed during hydraulic fracturing experiments at the Fenton Hill hot dry rock geothermal energy site, New Mexico. Int. J. Rock Mech. Min. Sci. Geomech. Abstr. 26, 211–219, http://dx.doi.org/10.1016/0148-9062(89)91971-2

Frye, K.M., Marone, C., 2002. Effect of humidity on granular friction at room temperature. J. Geophys. Res. Earth, 107, http://dx.doi.org/10.1029/2001jb000654, Artn 2309.

Gu, J.-C., Rice, J.R., Ruina, A.L., Tse, S.T., 1984. Slip motion and stability of a single degree of freedom elastic system with rate and state dependent friction. J. Mech. Phys. Solids 32, 167–196, http://dx.doi.org/10.1016/0022-5096(84)90007-3

Heidbach, O., Tingay, M., Barth, A., Reinecker, J., Kurfeß, D., Müller, B., 2010. Global crustal stress pattern based on the World Stress Map database release 2008. Tectonophysics 482, 3–15, http://dx.doi.org/10.1016/j.tecto.2009.07.023

Hubbert, M.K., Rubey, W.W., 1959. Role of fluid pressure in mechanics of overthrust faulting. I. Mechanics of fluid-filled porous solids and its application to overthrust faulting. Geol. Soc. Am. Bull. 70, 115–166.

Ikari, M.J., Marone, C., Saffer, D.M., 2011. On the relation between fault strength and frictional stability. Geology 39, 83–86, http://dx.doi.org/10.1130/g31416.1

Izadi, G., Elsworth, D., 2013. The effects of thermal stress and fluid pressure on induced seismicity during stimulation to production within fractured reservoirs. Terra Nov. 25, 374–380, http://dx.doi.org/10.1111/ter.12046

Kohli, A.H., Zoback, M.D., 2013. Frictional properties of shale reservoir rocks. J. Geophys. Res. Earth 118, 5109–5125, http://dx.doi.org/10.1002/Jgrb.50346

Lachenbruch, A.H., 1980. Frictional heating, fluid pressure, and the resistance to fault motion. J. Geophys. Res., http://dx.doi.org/10.1029/JB085iB11p06097

Lee, M.K., Wolf, L.W., 1998. Analysis of fluid pressure propagation in heterogeneous rocks: Implications for hydrologically-induced earthquakes. Geophys. Res. Lett. 25, 2329–2332, http://dx.doi.org/10.1029/98gl01694

Li, Y., Wang, J., Jung, W., Ghassemi, A.,2012. Mechanical properties of intact rock and fractures in welded tuff from Newberry Volcano. In: Thirty-Seventh Workshop on Geothermal Reservoir Engineering. Stanford University, Stanford, CA, p. 12.

Majer, E.L., Baria, R., Stark, M., Oates, S., Bommer, J., Smith, B., Asanuma, H., 2007. Induced seismicity associated with enhanced geothermal systems. Geothermics 36, 185–222, http://dx.doi.org/10.1016/j.geothermics.2007.03.003

Majer, E.L., Peterson, J.E., 2007. The impact of injection on seismicity at The Geysers, California Geothermal Field. Int. J. Rock Mech. Min. Sci. 44, 1079–1090, http://dx.doi.org/10.1016/j.ijrmms.2007.07.023

Marone, C., 1997. On the rate of frictional healing and the constitutive law for time- and slip-dependent friction. Int. J. Rock Mech. Min. Sci. Geomech. Abstr. 34, 347, http://dx.doi.org/10.1016/S1365-1609(97)00054-3

Marone, C., 1998. Laboratory-derived friction laws and their application to seismic faulting. Annu. Rev. Earth Planet. Sci. 26, 643–696, http://dx.doi.org/10.1146/Annurev.Earth.26.1.643

Niemeijer, A., Collettini, C., 2013. Frictional properties of a low-angle normal fault under in situ conditions: thermally-activated velocity weakening. Pure Appl. Geophys., 1–24, http://dx.doi.org/10.1007/s00024-013-0759-6

Petty, S., Nordin, Y., Glassley, W., Cladouhos, T.T., Swyer, M.,2013. Improving geothermal project economics with multi-zone stimulation: results from the Newberry Volcano EGS demonstration. In: PROCEEDINGS, Thirty-Eighth Workshop on Geothermal Reservoir Engineering. Stanford University, Stanford, CA.

Pine, R.J., Ledingham, P., Merrifield, C.M., 1983. In-situ stress measurement in the Carnmenellis granite. II. Hydrofracture tests at Rosemanowes quarry to depths of 2000 m. Int. J. Rock Mech. Min. Sci. Geomech. Abstr. 20, 63–72, http://dx.doi.org/10.1016/0148-9062(83)90328-5

Raleigh, C.B., Healy, J.H., Bredehoeft, J.D., 2013. Faulting and crustal stress at Rangely, Colorado. In: Flow and Fracture of Rocks. American Geophysical Union, pp. 275–284, http://dx.doi.org/10.1029/GM016p0275

Ruina, A., 1983. Slip instability and state variable friction laws. J. Geophys. Res. Solid Earth 88, 10359–10370, http://dx.doi.org/10.1029/JB088iB12p10359

Rutqvist, J., Freifeld, B., Min, K.B., Elsworth, D., Tsang, Y., 2008. Analysis of thermally induced changes in fractured rock permeability during 8 years of heating and cooling at the Yucca Mountain Drift Scale Test. Int. J. Rock Mech. Min. Sci. 45, 1373–1389, http://dx.doi.org/10.1016/j.ijrmms.2008.01.016

Samuelson, J., Marone, C., Voight, B., Elsworth, D., 2008. Laboratory investigation of the frictional behavior of granular volcanic material. J. Volcanol. Geotherm. Res. 173, 265–279, http://dx.doi.org/10.1016/j.jvolgeores.2008.01.015

Scholz, C.H., 1998. Earthquakes and friction laws. Nature 391, 37–42, http://dx.doi.org/10.1038/34097

Scholz, C.H., 2002. The Mechanics of Earthquakes and Faulting, 2nd ed. Cambridge University Press.

Shapiro, S.A., Huenges, E., Borm, G., 1997. Estimating the crust permeability from fluid-injection-induced seismic emission at the KTB site. Geophys. J. Int. 131, F15–F18, http://dx.doi.org/10.1111/J.1365-246x.1997.Tb01215.X

Shapiro, S.A., Rothert, E., Rath, V., Rindschwentner, J., 2002. Characterization of fluid transport properties of reservoirs using induced microseismicity. Geophysics, http://dx.doi.org/10.1190/1.1451597

Spada, M., Tormann, T., Wiemer, S., Enescu, B., 2013. Generic dependence of the frequency-size distribution of earthquakes on depth and its relation to the strength profile of the crust. Geophys. Res. Lett. 40, 709–714, http://dx.doi.org/10.1029/2012gl054198

Starr, A.T., 1928. Slip in a crystal and rupture in a solid due to shear. Math. Proc. Camb. Philos. Soc. 24, 489–500, http://dx.doi.org/10.1017/S0305004100014626

Stein, R.S., King, G.C., Lin, J., 1992. Change in failure stress on the southern San Andreas fault system caused by the 1992 magnitude = 7.4 Landers earthquake. Science 258, 1328–1332, http://dx.doi.org/10.1126/science.258.5086.1328

Tester, J., 2007. The Future of Geothermal Energy: Impact of Enhanced Geothermal Systems (EGS) on the United States in the 21st Century. MIT.

Townend, J., Zoback, M.D., 2000. How faulting keeps the crust strong. Geology 28, 399–402, http://dx.doi.org/10.1130/0091-7613(2000)28<399:HFKTCS>2.0.CO

Verberne, B.A., Spiers, C.J., Niemeijer, A.R., De Bresser, J.H.P., De Winter, D.A.M., Plümper, O., 2014. Frictional properties and microstructure of calcite-rich fault gouges sheared at sub-seismic sliding velocities. Pure Appl. Geophys. 171, 2617–2640, http://dx.doi.org/10.1007/s00024-013-0760-0

Zoback, M.D., Harjes, H.-P., 1997. Injection-induced earthquakes and crustal stress at 9 km depth at the KTB deep drilling site, Germany. J. Geophys. Res. Solid Earth 102, 18477–18491, http://dx.doi.org/10.1029/96JB02814

Zoback, M.D., Healy, J.H., 1992. In situ stress measurements to 3.5 km depth in the Cajon Pass Scientific Research Borehole: implications for the mechanics of crustal faulting. J. Geophys. Res., http://dx.doi.org/10.1029/91JB02175.